nature portfolio

Peer Review File

Sub-millimeter fiberscopic robot with integrated maneuvering, imaging, and biomedical operation abilities

Corresponding Author: Professor Yajing Shen

This file contains all reviewer reports in order by version, followed by all author rebuttals in order by version.

Version 0:

Reviewer comments:

Reviewer #1

(Remarks to the Author)
The authors developed a fiberscopic robot achieving the combination of small size, motion control and multi-functions, which was termed as an “impossible trinity”. This manuscript presented an impressive number of interesting engineering design innovations, results, and characterizations.

My major comment is about the imaging quality of the fiber optic robot, which looks quite limited, according to Fig. 5(b2) and Supplementary videos. Please comment on how to improve. Is it due to the small size. Sup S16 shows decent resolution, but what about the image contrast? How does the contrast and resolution of this device compare to clinically used endoscopes?

Below are my minor comments to help the authors improve the manuscript:
1. In the abstract, the authors wrote “… extends obstacle detection distance up to ~9.4 mm, a tenfold improvement from the theoretical limits”. However, this point was not explained enough in the results. Did the authors mean the theoretical limit shown in Fig. 3(c)? Was the ‘tenfold improvement’ calculated by comparing dashed line in Fig. 3(c) to the dashed line in Fig. 3(f)? In addition, how did the authors get ‘~9.4mm’? what about 9.5mm?
2. The authors wrote “the optical fiber-based probe can be made very small and can either provide imaging (e.g., microstructure investigation inside the arteries (19-22))” However, Reference 19-21 didn’t show imaging inside arteries. If the authors would like to cite these papers, please edit this sentence to correctly indicate what these references have demonstrated.
3. Figure 1 looks too busy, especially the Fig. 1(b). There are many labels but very small gaps between the sub figure b and other sub figures.
4. Figure 3: please explain in the figure legend what are the dashed line in sub figures Fig. 3(c) and (f) mean. In addition, please explain “TL” “TR” “BL” “BR” in the figure legend to make it easier for readers to understand the figure without searching in the main manuscript.
5. Figure 4 (c) (d) (e), what are the blue, green dots representing? Please include a short description about them in the figure legend or main text.
6. The authors wrote: “three standard light guide fibers with 125 μm diameter (IR105/125-AC, Fibestar Technology Co., Ltd., Beijing, China), and one functional tool (micro tube with an outer/inner diameter of 100/50 μm, or laser fiber with 125 μm diameter). Are these fibers with coating/buffer? How fragile are they? What’s their minimal bending radius? If they cannot be bend sharp enough due to the lack of coating/buffer, they probably would limit the application of the reported novel fiberoptic robot.
7. Discussion: the authors wrote “Leveraging the probe’s high-precision motion, we proposed a strategy of local scanning and stitching, enlarging the overall imaging region by ~25 folds. This strategy not only enhances the diagnostic potential of the robot through scanning imaging of pathological areas but also opens up possibilities for precise in situ surgical manipulations”. This method of local scanning and stitching has its advantages, but it may also slow down the scanning speed and/or be prone to motion artifact (i.e., stitching may not work well when there is strong breathing or cardiac motion artifact). Please comment on the limitations of this stitching technique in the discussion section.

Reviewer #3

(Remarks to the Author)
This study presents a continuous fiber optic robot capable of performing high-precision movements while enabling multifunctional operations. The main innovation is the integration of microscopic 3D printing technology and magnetic spraying to achieve a robot with a very small diameter. This robot overcomes traditional limitations related to size, accurate navigation, and functional visualization ("impossible trinity"). It can navigate constrained environments and perform tasks such as imaging, diagnostics, drug delivery, and laser ablation.

Experimental results demonstrate that the robot can navigate precisely within narrow environment and perform various procedures, including biopsy, drug delivery, and laser ablation. The robot's performance, measured in terms of positioning accuracy and procedural efficiency, shows an improvement over previous devices. This work has significant implications for the development and design of a submillimeter-scale robot that combines imaging, navigation, and surgical capabilities, thereby addressing the main limitations of minimally invasive operations.

The data and methodology are presented with great clarity and detail. However, here are a few comments/questions regarding the manufacturing procedure:

- Adding information on the variability of manufacturing results (reproducibility, dimensional tolerances, observed defects, etc...) could provide a more comprehensive overview of the process

- The mentioned materials (especially photosensitive resins and elastomers) could benefit from more details regarding their specifications (long-term stability, biocompatibility, etc...)

- Spraying can lead to variations in thickness and thus create a non-uniform distribution of ferromagnetic particles (which would consequently affect the overall magnetic properties). Is there a specific method for spraying ?

- The ultrafine fillets of 80 µm exhibit mechanical weaknesses. In figure S4, under mechanical loads, I would expect to see "failures" at this level. Could you explain why this is not the case?

- The assembly procedure is briefly mentioned, but additional details could be beneficial (difficulties encountered during the insertion of components into the skeleton holes, methods to ensure assembly precision, etc...)

- The assembly is finalized by applying UV glue. Has this fixation been tested under different conditions, particularly humidity, which is a significant factor in a clinical context ?

The analytical approach employed in this study is robust, with appropriate use of methods to evaluate the robot's performance. The authors use statistical methods to analyze the data obtained during the robot's performance tests, particularly concerning navigation accuracy and the efficiency of the imaging system. The experimental results show good agreement with the theoretical analyses, which reinforces the validity of the conclusions

Version 1:

Reviewer comments:

Reviewer #1

(Remarks to the Author)
The authors have addressed most of my comments. The only final comment I have is for the authors to double check this newly added sentence: "Despite the reported stitching approach would slow down the
scanning speed and be prone to body's movements". This sentence is a bit confusing. Did you mean, "Despite these advantages, the reported stitching approach would slow down the
scanning speed and be prone to body's movements".

Reviewer #3

(Remarks to the Author)
I would like to thank the authors for their detailed responses to my previous comments. The points raised have been addressed appropriately, and the revisions made to the manuscript (Supplementary Materials) seem coherent to me.

Reviewer #1 (Remarks to the Author):

The authors developed a fiberscopic robot achieving the combination of small size, motion control and multi-functions, which was termed as an "impossible trinity". This manuscript presented an impressive number of interesting engineering design innovations, results, and characterizations.

Response:

Thanks for your positive comments on our work.

My major comment is about the imaging quality of the fiber optic robot, which looks quite limited, according to Fig. 5(b2) and Supplementary videos. Please comment on how to improve. Is it due to the small size. Sup S16 shows decent resolution, but what about the image contrast? How does the contrast and resolution of this device compare to clinically used endoscopes?

Response:

Thanks for your insightful comments. The imaging quality of the fiberscopic robot and the improvement methods are discussed below:

(1) Resolution: Our fiberscopic robot is capable of achieving a high resolution with an error of about 2 μm, as the results in Fig. S16/17. This performed imaging resolution surpasses that of most clinically used endoscopes, which typically with a resolution of about 10 μm (cellular/subcellular resolution)[1][2].

(2) Contrast: As shown in Figures S13 and S14, our fiberscopic robot can capture the edges of the symbol '5' with noticeable contrast against its surroundings. However, there is currently no standard method to quantitatively evaluate image contrast in endoscopes, preventing us from making comparisons at this stage. To further improve image quality, we can adjust the exposure parameters. For instance, image contrast is low when the overall intensity is either too weak or too strong at exposure durations of 5 ms or 30 ms, respectively. The symbol '5' can be captured with a clearer contour at an intermediate exposure duration. Another method to enhance image contrast is by optimizing the image processing algorithms. In future work, we plan to develop a system that includes an automatic adjustment algorithm for exposure duration and image processing procedures to advance the clinical application of our proposed fiberscopic robot.

In this revised version, we have discussed the image resolution and contrast in the Supplementary text. Please see the following modifications.

Modifications: (Supplementary Note S6.2)

In short, the proposed probe and the corresponding endoscopic imaging system can achieve competitive imaging performance for microscale object, e.g., setting the exposure duration of the camera as 10 ms, we can achieve a better contour segmentation within a long distance and the capture error low to ~2.0 μm for the target. The performed imaging resolution surpasses that of most clinically used endoscopes, which typically with a resolution of about 10 μm (cellular/subcellular resolution)[13,14]. Besides, to improve the captured image contrast, we can either set a proper exposure parameter or optimize the image processing algorithms. In the future work, we plan to develop a

system that includes an automatic adjustment algorithm for exposure duration and image processing procedures to advance the clinical application of our proposed fiberscopic robot.

Below are my minor comments to help the authors improve the manuscript:

1. In the abstract, the authors wrote "… extends obstacle detection distance up to ~9.4 mm, a tenfold improvement from the theoretical limits". However, this point was not explained enough in the results. Did the authors mean the theoretical limit shown in Fig. 3(c)? Was the 'tenfold improvement' calculated by comparing dashed line in Fig. 3(c) to the dashed line in Fig. 3(f)? In addition, how did the authors get '~9.4mm'? what about 9.5mm?

Response:

Thanks for your kind comments on the obstacle detection distance. Please find the reply item by item as below:

(1) Theoretical limit: Based on both theoretical and experimental results, the collected light flux by the probe reaches its maximum value at a distance of approximately 1 mm (Figures 3c and 3d), indicating a state of complete overexposure. Therefore, we define this distance as the theoretical limit for clear imaging, beyond which it is impossible to recognize any objects distinctly.

(2) Detection distance of 9.4 mm: As shown in Fig. S9a, we placed a reflective board in front and moved it from near to far while collecting the light intensity from the central fiber bundle. The experimental results show that we can still recognize the rough orientation of an object in front, specifically in the top left direction, at a distance of ~9.4 mm, shown in Fig. 3f. It is the farthest distance we can achieve obstacle detection. (The detailed description of the experimental results can be found in supplementary note S6.1 and Fig. S11.)

(3) Ten-folds improvement: By comparing the experimentally measured object detection distance of ~9.4 mm with the theoretical limit of ~1.0 mm, we describe such an extension as a tenfold improvement.

In this revised version, we have added more description in the main text to explain such results. Please see the following modifications.

Modifications: (Part "Interventional imaging and out-of-sight navigation inside narrow channel" of Section Results)

To achieve effective and safe steering, the exploration ability in a farther region than the theoretical maximum imaging distance (1mm) is also essentially significant for identifying the branches and obstacles to make proper decisions (e.g., entrance or bypass) in advance. To address this challenge, we proposed an intensity distribution-based environment exploration strategy and extended the blur obstacle detection distance approximately 10 folds farther to ~9.4 mm (see supplementary note S6.1 for detail). As illustrated in Fig. 3e, when an object is offset placed in front, the collected light through the central fiber bundle is different, i.e., the intensity will be higher if the object is positioned in this quadrant, or will be lower if a free channel is in front. Thus, we can take the collected intensity as the parameter to forecast the environment though there is no clear image. To demonstrate it, we divide the endoscopic view into four

quadrants, i.e., top left (TL), top right (TR), bottom left (BL), and bottom right (BR) (Fig. 3e). By analyzing the variation of both the separate intensity and the corresponding normalized value from the four quadrants, we can not only identify whether there is an obstacle in front but also estimate its relative orientation to the probe. For instance, an object with a 0.5 mm lateral offset while at a distance of about 9.4 mm can still have its rough orientation estimated as being in the top left quadrant, based on the fact that the normalized intensity in this quadrant exceedes the threshold (Fig. 3f, supporting Fig. S13, supplementary note S6.1).

2. The authors wrote "the optical fiber-based probe can be made very small and can either provide imaging (e.g., microstructure investigation inside the arteries (19-22))" However, Reference 19-21 didn't show imaging inside arteries. If the authors would like to cite these papers, please edit this sentence to correctly indicate what these references have demonstrated.

Response:

Thanks for your kind advice. We previously classified the references 19-22 as the same technology for utilizing optical fiber to provide imaging. And for the application in arteries, there is only reference 22 shown.

In the revised version, we have corrected this sentence to avoid any misunderstanding. Please see the following modifications.

Modifications: (The second paragraph of Section Introduction)

The optical fiber-based probe can be made very small and can either provide imaging (*19-21*) (e.g., microstructure investigation inside the arteries(*22*)) or surgical functions (e.g., laser delivery/ablation(*23, 24*)).

3. Figure 1 looks too busy, especially the Fig. 1(b). There are many labels but very small gaps between the sub figure b and other sub figures.

Response:

Thanks for your kind advice. We have already reorganized Figure 1 to obtain a better understanding in the revised version. Please see the following modifications.

Modifications: (Part "Design and fabrication of the submillimeter robotic probe by 3D printing and magnetic spray" of Section Results)

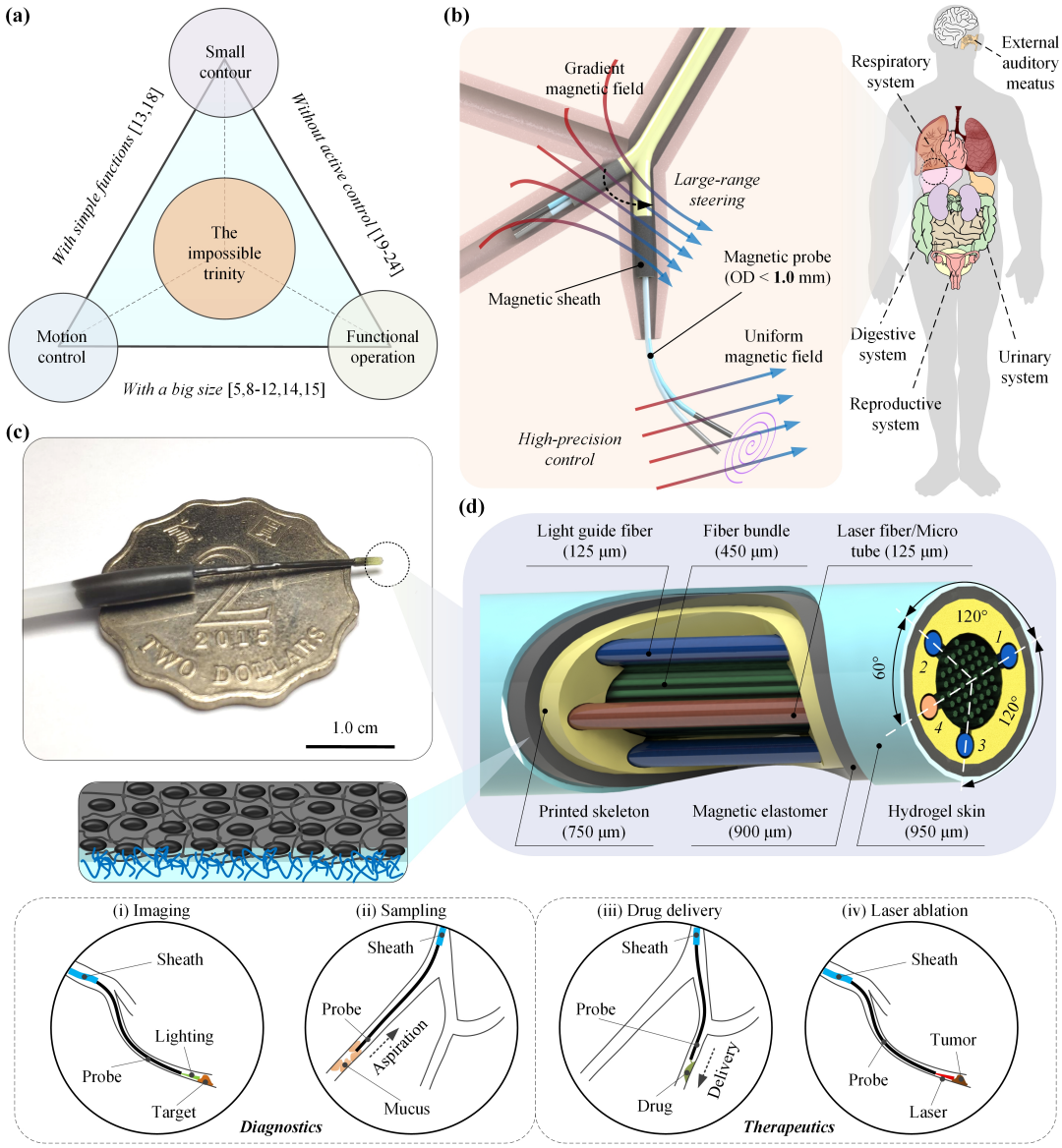

Figure R1. Overview of the optical fiber-based sub-millimeter continuum robot with imaging, maneuvering, and medical operation capabilities. (a) Achieving small contour, high-precision motion control, and visualized functional operations simultaneously poses a challenge for robots, referred to as the "impossible trinity". (b) Schematics of the proposed sub-millimeter continuum robot driven by multi-sectional magnetic fields for medical diagnosis and treatment in narrow channels. (c) Image depicting the probe tip, over a two-dollar Hong Kong coin. (d) Schematic of the probe tip, comprising of a central fiber bundle, three light guide fibers (No. 1, 2, 3), and an additional functional tool channel (No. 4) within the skeleton fabricated by microscale 3D printing technology. A thin layer of magnetic elastomer is coated on the probe for actuation, and then a thin hydrogel layer is covered on the outer surface to reduce the friction. The manufactured probe boasts a diameter contour of 0.95 mm. The diagnostic and therapeutic potential of the fiberscopic robot include (i) imaging, (ii) sampling, (iii) drug delivery, and (iv) laser ablation.

4. Figure 3: please explain in the figure legend what are the dashed line in sub figures Fig. 3(c) and (f) mean. In addition, please explain "TL" "TR" "BL" "BR" in the figure legend to make it easier for readers to understand the figure without searching in the main manuscript.

Response:

Thanks for your kind advice. We have improved the caption description for Figure 3 to obtain a better understanding. Please see the following modifications.

Modifications: (Part "Interventional imaging and out-of-sight navigation inside narrow channel" of Section Results)

Figure 3. Imaging system characterization of the probe. (a) Schematic representation of the endoscopic imaging system and the depiction of the corresponding imaging zone and assisted navigation zone in front of the probe. Results illustrate the capture of number symbol "5" within the imaging zone, and the detect of an obstacle positioned beyond the imaging zone. (b) Illustration of the transmission principle of light intensity distribution through the proposed probe, with a reflective board positioned at a distance ds and an offset *dr* from the probe tip and its central plane, respectively. (c) Theoretical representation of the light intensity collected by the central fiber bundle against distance *ds* and lateral offset *dr* of the reflective board. The dashed line denotes the theoretical limit of imaging clearly. (d) Experimental measurement of the collected light intensity against distance ds and lateral offset *dr* of the reflective board, exhibiting a similar trend with the theoretical one. (e) The principle of the proposed intensity distribution-based environment exploration strategy for identifying objects beyond the imaging zone, e.g., an evenly normalized intensity of 0.25 would be obtained for the four quadrants if a reflective obstacle fully covers the probe tip. (f) Analytical evidence confirming the existence and orientation of the object beyond the imaging zone with an offset of 0.5 mm. The normalized intensity from the TL quadrant is ~0.33 at a distance of ~9.4 mm, indicating an obstacle in the top left direction in front of the probe, despite being out-of-sight. TL, TR, BL, and BR represent top left, top right, bottom left, and bottom right, respectively. The dashed line on the corner denotes the farthest distance of ~9.4 mm, where an object in front can still be estimated the relative orientation.

5. Figure 4 (c) (d) (e), what are the blue, green dots representing? Please include a short description about them in the figure legend or main text.

Response:

Thanks for your kind advice. We have improved the caption description for Figure 4 to obtain a better understanding. Please see the following modifications.

Modifications: (Part "High precise positioning, image scanning and stitching based on multi-sectional magnetic steering" of Section Results)

Figure 4. High precise maneuvering of the continuum robot. (a) Schematic depicting the multi-sectional actuation by the magnetic field. The magnetic sheath is actuated by a gradient magnetic field to achieve large-range steering, while the magnetic probe is actuated by a uniform magnetic field to achieve high-precision motion. (b) Experimental setup for evaluating the probe's motion trajectory. (c-e) Path tracking results of the probe tip under square (c), circle (d), and spiral (e) trajectories, presenting

a motion error of less than 30 μm for complex 3D trajectories. The light blue, green, and purple dots here correspond to the projection in the x-o-y plane, x-o-z plane, and y-o-z plane of the recorded trajectories. (f) Schematic illustrating sample scanning by a designed Archimedes spiral trajectory. (g) Reconstruction results (one leaf of a Bauhinia flower) utilizing the local scanning and stitching strategy, achieving a ~25-fold expansion of view. (h) Schematic of the interventional procedure performed by the continuum robot in an in vitro bronchial tree model. (i) Experimental snapshot of the interventional process and the scanning result of a grid pattern.

6. The authors wrote: "three standard light guide fibers with 125 μm diameter (IR105/125-AC, Fibestar Technology Co., Ltd., Beijing, China), and one functional tool (micro tube with an outer/inner diameter of 100/50 μm, or laser fiber with 125 μm diameter). Are these fibers with coating/buffer? How fragile are they? What's their minimal bending radius? If they cannot be bend sharp enough due to the lack of coating/buffer, they probably would limit the application of the reported novel fiberoptic robot.

Response:

Thanks for your insightful comments. Please find the reply item by item as below:

(1) Are these fibers with coating/buffer? When fabricating the submillimeter probe, we removed the outer coating/buffer layer of the optical fiber (Fig R2, OD: 220 μm) while preserving the glass core and glass cladding (OD: 125 μm). The fiber type of 105/125 correspondingly denotes the diameter of the glass core/cladding.

(2) The fragile and minimal bending radius: We tested the minimal bending radius of the optical fiber at about 3.38 mm without the outer coating layer, as shown in Fig R3a.

(3) Sharp enough for real application? To protect the fiber array, we coated the outer surface of the long rear body of the probe robot with a thin layer of elastomer and hydrogel skin (Fig. 1, Fig. S1). In this case, the assembled probe robot can still show a small bending radius of about 5.58 mm (Fig R3b). This value is about five times smaller than most of the reported traditional endoscopes (~30 mm)[3]-[5] and even smaller than that of the ultra-fine micro borescope (~ 6.0 mm) [6][7]. Consequently, the fabricated probe robot can show its bright application potential in practical scenarios.

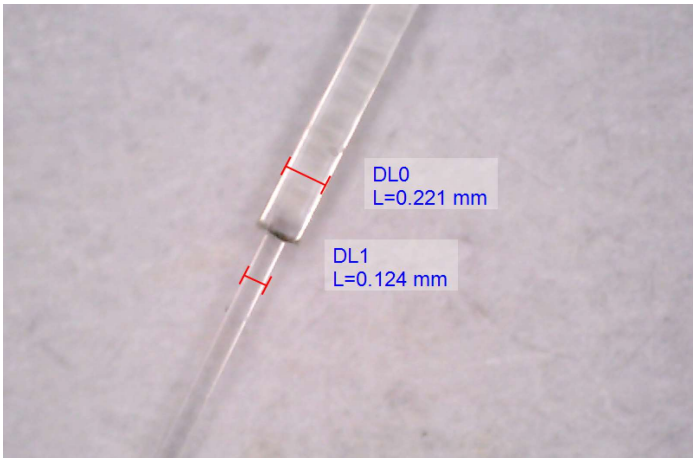

Figure R2. Contour measurement of the optical fiber utilized for transmitting medical cold light and the ablation laser.

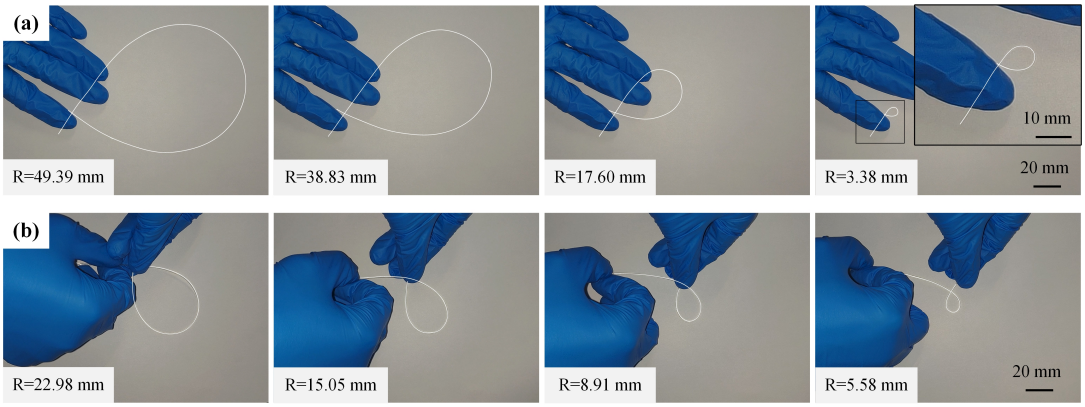

Figure R3. Bending performance of the optical fiber and the probe robot. (a-b) The bending performance of the optical fiber without the outer coating layer(a), and the assembled probe robot(b).

In this revised version, we have added more description in the supplementary file to explain such results. Please see the following modifications.

Modifications: (Supplementary Note S1)

Fragile performance: As for the fragile performance, we utilized the bare optical fiber with the glass core and glass cladding (OD: 125 μm) while removing the outer coating/buffer layer (Fig. S2, OD: 220 μm) and tested the minimal bending radius of the optical fiber at about 3.38 mm, as shown in Fig. S3a. To protect the fiber array, we coated the outer surface of the long rear body of the probe robot with a thin layer of elastomer and hydrogel skin (Fig. 1, Fig. S1). In this case, the assembled probe robot can still show a small bending radius of about 5.58 mm (Fig. S3b). This value is about five times smaller than most reported traditional endoscopes (~30 mm)[9-11] and even smaller than that of the ultra-fine micro borescope(~ 6.0 mm) [12,13]. Consequently, the fabricated probe robot can show its bright application potential in practical scenarios.

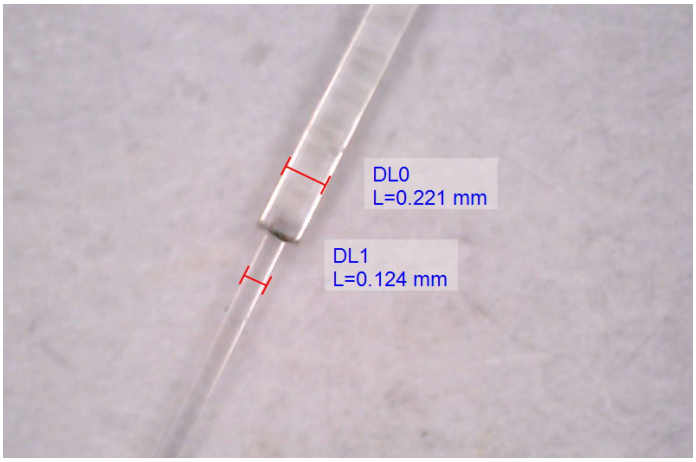

Figure S2. Contour measurement of the optical fiber utilized for transmitting medical cold light and the ablation laser.

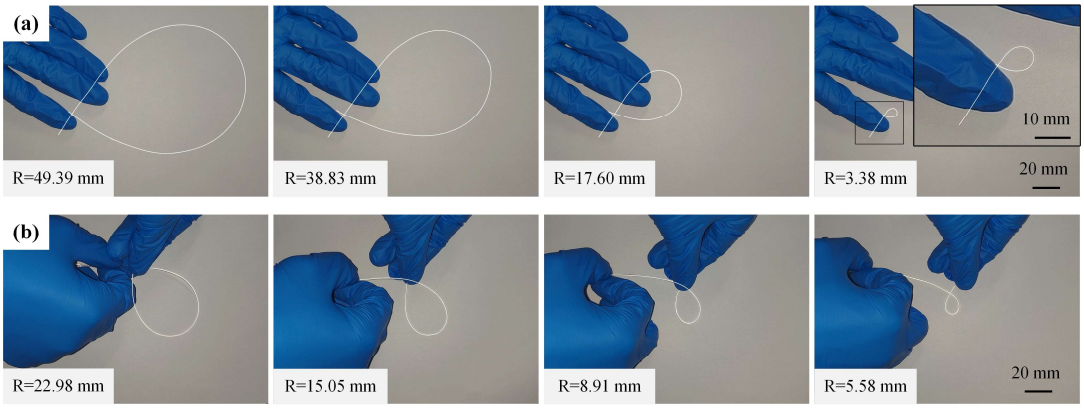

Figure S3. Bending performance of the optical fiber and the probe robot. (a-b) The bending performance of the optical fiber without the outer coating layer(a), and the assembled probe robot(b).

7. Discussion: the authors wrote "Leveraging the probe's high-precision motion, we proposed a strategy of local scanning and stitching, enlarging the overall imaging region by ~25 folds. This strategy not only enhances the diagnostic potential of the robot through scanning imaging of pathological areas but also opens up possibilities for precise in situ surgical manipulations". This method of local scanning and stitching has its advantages, but it may also slow down the scanning speed and/or be prone to motion artifact (i.e., stitching may not work well when there is strong breathing or cardiac motion artifact). Please comment on the limitations of this stitching technique in the discussion section.

Response:

We acknowledge your comments regarding the stitching approach potentially slowing down the scanning speed and being susceptible to body movements. In this manuscript, we have demonstrated the feasibility of this approach for enlarging the imaging area. In future work, we will address this challenge by: (1) optimizing the image processing algorithm to enhance stitching efficiency; (2) designing the scanning path as a denser spiral trajectory with smaller gaps between adjacent curves to minimize information loss; and (3) upgrading the stitching algorithm by integrating both trajectory and image features to improve accuracy.

We have added the corresponding comments about the stitching approach in the discussion section. Please see the following modifications.

Modifications: (The second paragraph of Section Discussion)

Due to the inherent contour limitation of the fiber bundle, the field of vision of existing fiber-based imaging systems usually cannot provide sufficient information on the pathological area. Leveraging the probe's high-precision motion, we proposed a strategy of local scanning and stitching, enlarging the overall imaging region by ~25 folds. This strategy can not only enhance the diagnostic potential of the robot through scanning imaging of pathological areas but also open up possibilities for precise in situ surgical manipulations. Despite the reported stitching approach would slow down the

scanning speed and be prone to body's movements. In this manuscript, we have demonstrated the feasibility of this approach for enlarging the imaging area. In future work, we will address this challenge by: optimizing the image processing algorithm to enhance stitching efficiency; designing the scanning path as a denser spiral trajectory with smaller gaps between adjacent curves to minimize information loss; and upgrading the stitching algorithm by integrating both trajectory and image features to improve accuracy.

Reviewer #3 (Remarks to the Author):

This study presents a continuous fiber optic robot capable of performing high-precision movements while enabling multifunctional operations. The main innovation is the integration of microscopic 3D printing technology and magnetic spraying to achieve a robot with a very small diameter. This robot overcomes traditional limitations related to size, accurate navigation, and functional visualization ("impossible trinity"). It can navigate constrained environments and perform tasks such as imaging, diagnostics, drug delivery, and laser ablation.
Experimental results demonstrate that the robot can navigate precisely within narrow environment and perform various procedures, including biopsy, drug delivery, and laser ablation. The robot's performance, measured in terms of positioning accuracy and procedural efficiency, shows an improvement over previous devices. This work has significant implications for the development and design of a submillimeter-scale robot that combines imaging, navigation, and surgical capabilities, thereby addressing the main limitations of minimally invasive operations.
The data and methodology are presented with great clarity and detail.

Response:
Thanks for your positive comments on our work.

However, here are a few comments/questions regarding the manufacturing procedure:
- Adding information on the variability of manufacturing results (reproducibility, dimensional tolerances, observed defects, etc...) could provide a more comprehensive overview of the process

Response:
Thanks for your kind advice. The manufacturing results is quite reliable if the fabrication process can be strictly followed. The measured diameter ranges of the printed skeleton, the magnetic elastomer, and the hydrogel skin are about 740-760μm, 880-920μm, and 940-960 μm, respectively, showing a good uniformity. To help the researcher reproduce these results, here we list some key points needed to pay attention during the fabrication:
(1) Due to the hollow structure, the printed skeleton may encounter geometrical deformation during the printing procedure. It is necessary to attach enough detachable supports to the structure in the slicing software.
(2) Due to the deep-hole structure, there could retain resin residues inside that induce difficulty in component insertion. Please check the residue and carry out further clean after the printing if necessary.
(3) During the assembly procedure of the fiber array, it is essential to manually insert slowly to prevent damage.
(4) After the successful insertion of the fiber array, each fiber would be slightly adjusted to achieve the parallel assembly.
We have added more detailed descriptions of the fabrication procedure in the supplementary text. Please see the following modifications.

Modifications: (Supplementary Note S1)

Supplementary Note S1. Additional information about the fabrication procedures

As shown in Fig. S1, the fabrication process of the proposed fiberscopic robot can be roughly divided into three main steps, including the main body construction (Fig. S1a,b), magnetic elastomer formation(Fig. S1c,d), and hydrogel skin generation(Fig. S1e,f). The overall manufacturing results are quite reliable if the fabrication process can be strictly followed.

(1) Fabrication details: To help the researcher reproduce this result, here we list some key points needed to pay attention during the fabrication.
a. Main body construction: (i) Due to the hollow structure, the printed skeleton may encounter geometrical deformation during the printing procedure. It is necessary to attach enough detachable supports to the structure in the slicing software. (ii) Due to the deep-hole structure, there could retain resin residues inside that induce difficulty in component insertion. Please check the residue and carry out further clean after the printing if necessary. (iii) During the assembly procedure of the fiber array, it is essential to manually insert slowly to prevent damage. (iv) After the successful insertion of the fiber array, each fiber would be slightly adjusted to achieve the parallel assembly.

(2) Dimensional tolerance: Regarding the dimensional tolerances of the entire manufacturing process, the measured diameter ranges of the printed skeleton, the magnetic elastomer, and the hydrogel skin are about 740-760μm, 880-920μm, and 940-960 μm, respectively, showing a good uniformity.

- The mentioned materials (especially photosensitive resins and elastomers) could benefit from more details regarding their specifications (long-term stability, biocompatibility, etc...)

Response:

Thanks for your insightful advice. The utilized photosensitive resins from BMF Material Technology Inc. are known as a type of material with long-term stability and biocompatibility, making them suitable for fabricating various biomedical devices[9]-[11]. Besides, the elastomer we used is also a common type of biocompatible silicone rubber that has been widely applied in fabrication of biomedical robots/devices[12]-[14]. Lastly, the hydrogel we employed has demonstrated the capability of antifouling and bacterial adhesion resistance[15].

We have added more detailed descriptions of the materials safety in the supplementary text. Please see the following modifications.

Modifications: (Supplementary Note S1)

Supplementary Note S1. Additional information about the fabrication procedures

Materials safety: Considering the safety utilization of the materials, the utilized photosensitive resins from BMF Material Technology Inc. are known as a type of material with long-term stability and biocompatibility, making them suitable for fabricating various biomedical devices [2-4]. Besides, the elastomer we utilized is also a common type of biocompatible silicone rubber that has been widely applied in fabrication of biomedical robots/devices[5-7]. Lastly, the hydrogel we employed has demonstrated the capability of antifouling and bacterial adhesion resistance [8].

Therefore, the utilized materials can well guarantee the safety.

- Spraying can lead to variations in thickness and thus create a non-uniform distribution of ferromagnetic particles (which would consequently affect the overall magnetic properties). Is there a specific method for spraying?

Response:

Thanks for your comments. We here utilize a self-developed technology of magnetic spray (*Science robotics, 5(48), eabc8191*) to generate the thin elastomer skin, which can provide a uniform result. Briefly, due to the viscosity of the elastomer matrix, the magnetic particles with several micrometers diameter can be well distributed to achieve a homogeneous status after the efficient stirring. With quick and high-pressure spraying, the obtained magnetic skin will achieve a relatively uniform state without affecting the overall magnetic properties. Besides, as described in the manuscript, the coating area of the robot tip is relatively short (~ 15 mm), so the sprayed elastomer skin would cause little impact on the actuation.

We have already added more detailed descriptions of the fabrication procedure in the supplementary text. Please see the following modifications.

Modifications: (Supplementary Note S1)

Supplementary Note S1. Additional information about the fabrication procedures

b. Magnetic elastomer formation: To form the magnetic elastomer, we here utilize a self-developed technology of magnetic spray[1]. (i) Due to the viscosity of the elastomer matrix, it is necessary to stir the mixture efficient to achieve a homogeneous status. (ii) With quick and high-pressure spraying, the obtained magnetic skin would obtain a relatively uniform state.

- The ultrafine fillets of 80 μm exhibit mechanical weaknesses. In figure S4, under mechanical loads, I would expect to see "failures" at this level. Could you explain why this is not the case?

Response:

Thanks for your insightful comments. As shown in Fig. R4b, the original thickness of the fillets is only 5 μm, resulting in low strength and fabrication difficulties. To improve the mechanical performance, we modified the skeleton structure by resecting the original ultrathin fillets (Fig. R4b) into parallel-plane types with an 80 μm width (Fig. R4a). As the results shown in Fig. R5, the modified skeleton structure shows a much better mechanical performance than the original one when subjecting the same normal/lateral/torsional load.

According to the FEM results shown in Fig. 2i/j/k, the modified skeleton structure would reach the strength limit under a normal/lateral/torsional load of about 15.7 N, 1.2 N, and 0.35 N/mm, respectively, which greatly exceeds the subjected load in clinical practice. Thus, the skeleton structure would not meet failure.

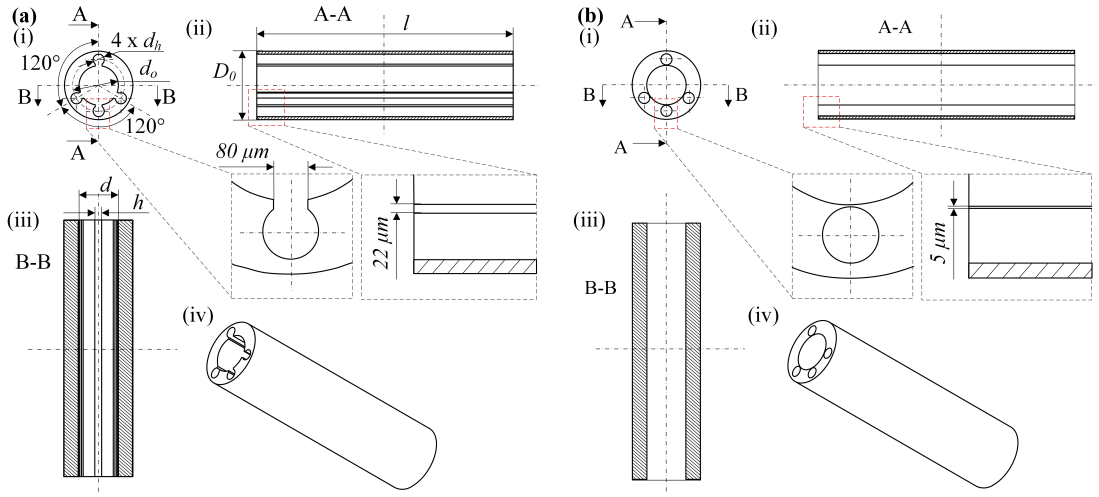

Figure R4. Structural comparison of the skeleton. (a,b) CAD model of the skeleton with(a)/without(b) fillets resection. (i) Top view of the skeleton. (ii) A-A section view of the skeleton. (iii) B-B section view of the skeleton. (iv) Axonometric view of the skeleton.

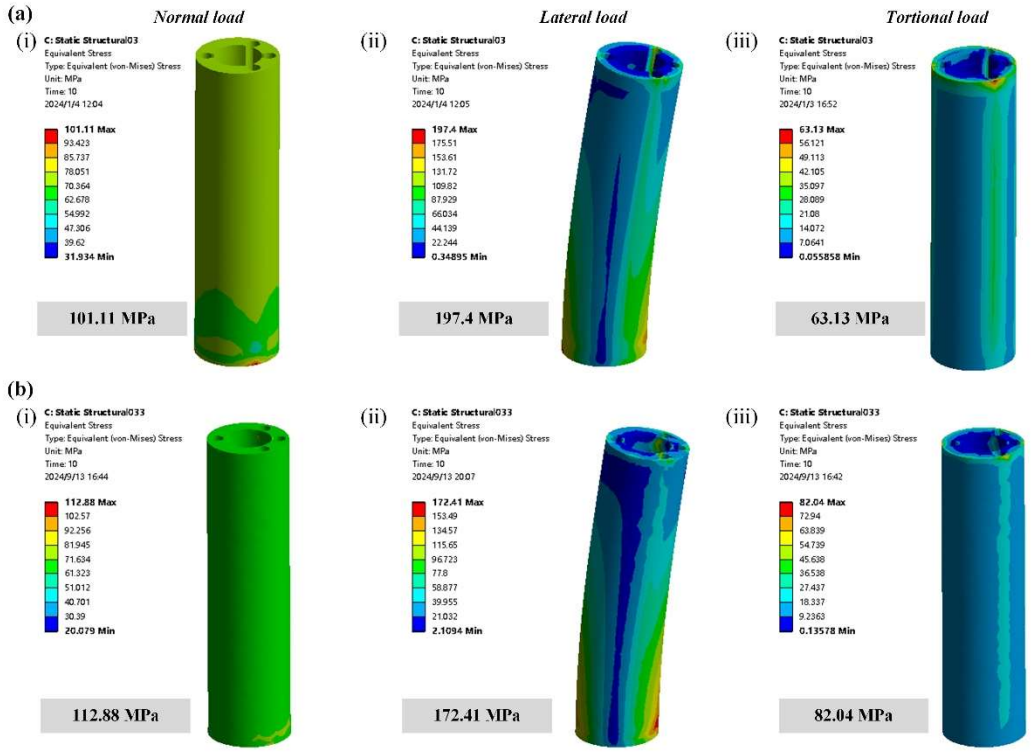

Figure R5. FEM mechanical simulation comparison of the skeleton. (a,b) FEM simulation results of the skeleton with(a)/without(b) fillets resection. (i) The result of the skeleton subjecting to a normal load of 20.0 N. (ii) The result of the skeleton subjecting to a lateral load of 2.0 N. (d) The result of the skeleton subjecting to a torque load of 0.5 N•mm.

We have already added more detailed descriptions of the mechanical design and analysis in the supplementary text. Please see the following modifications.

Modifications: (Supplementary Note S3)

Supplementary Note S3. Mechanical analysis for the skeleton

As stated in the materials and methods section, to address the challenges posed by the low strength and printing difficulties associated with the ultrathin fillets connecting the peripheral holes to the central lumen, we have modified the design by resecting these fillets into parallel planes.

To verify the necessity of the structural modification, we compared the mechanical performance of a skeleton with four peripheral holes with/without such resection.

As shown in Fig. S6b, the original thickness of the fillets is only 5 μm, resulting in low strength and fabrication difficulties. To improve the mechanical performance, we modified the skeleton structure by resecting the original ultrathin fillets into parallel-plane types with an 80 μm width (Fig. S6a). As the simulation results shown in Fig. S7, the modified skeleton structure shows a much better mechanical performance than the original one when subjecting the same normal/lateral/torsional load.

According to the FEM results shown in Fig. 2i/j/k, the modified skeleton structure would reach the strength limit under a normal/lateral/torsional load of about 15.7 N, 1.2 N, and 0.35 N/mm, respectively, which greatly exceeds the subjected load in clinical practice. Thus, the skeleton structure would not meet failure.

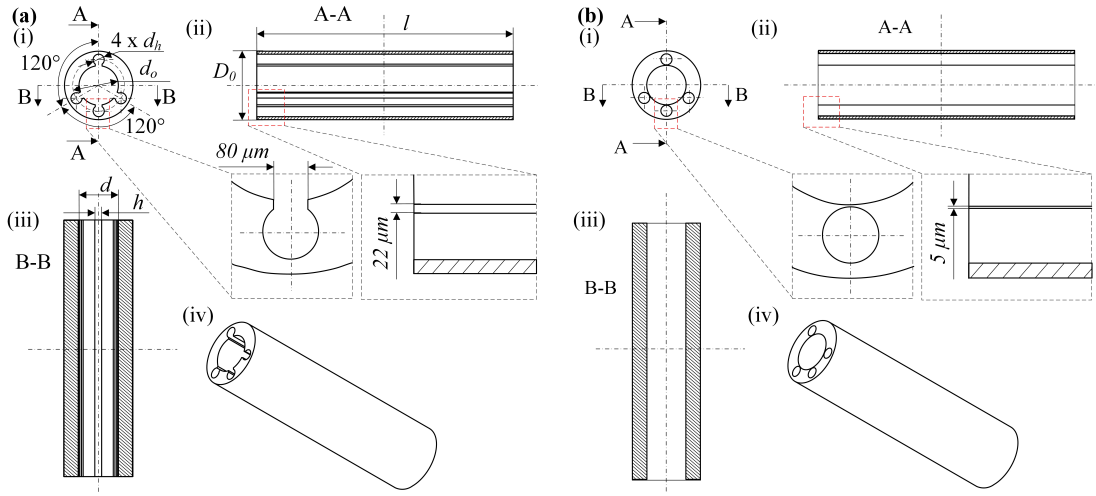

Figure S6. Structural comparison of the skeleton. (a,b) CAD model of the skeleton with(a)/without(b) fillets resection. (i) Top view of the skeleton. (ii) A-A section view of the skeleton. (iii) B-B section view of the skeleton. (iv) Axonometric view of the skeleton.

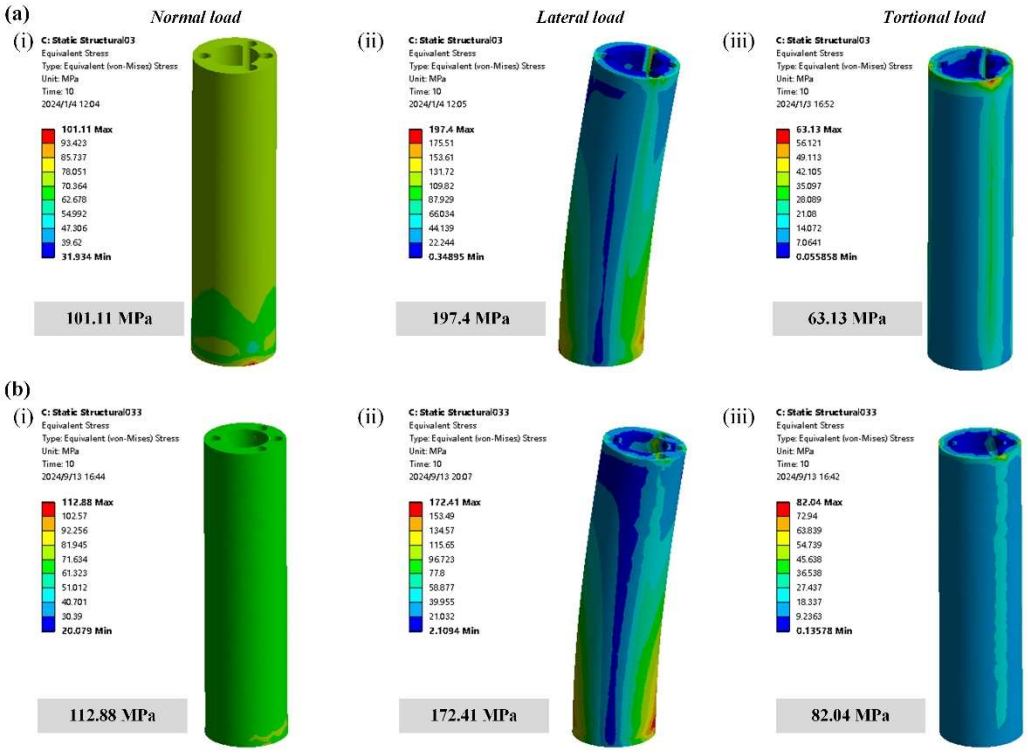

Figure S7. FEM mechanical simulation comparison of the skeleton. (a,b) FEM simulation results of the skeleton with(a)/without(b) fillets resection. (i) The result of the skeleton subjecting to a normal load of 20.0 N. (ii) The result of the skeleton subjecting to a lateral load of 2.0 N. (d) The result of the skeleton subjecting to a torque load of 0.5 N•mm.

- The assembly procedure is briefly mentioned, but additional details could be beneficial (difficulties encountered during the insertion of components into the skeleton holes, methods to ensure assembly precision, etc...)

Response:

Thanks for your kind advice. We have included more detailed descriptions of the fabrication procedure in the supplementary text, especially on the key steps that needed to pay attention. Briefly: (1) there could retain resin residues inside that induce difficulty in component insertion, so post cleaning should be conducted if necessary. (2) during the assembly procedure of the fiber array, it is essential to manually insert slowly to prevent damage. (3) after the successful insertion of the fiber array, each fiber would be slightly adjusted to ensure the parallel assembly.

Please see the following modifications.

Modifications: (Supplementary Note S1)

Supplementary Note S1. Additional information about the fabrication procedures

a. Main body construction: (i) Due to the hollow structure, the printed skeleton may encounter geometrical deformation during the printing procedure. It is necessary to attach enough detachable supports to the structure. (ii) Due to the deep-hole structure, there could retain resin residues inside that induce difficulty in component insertion. It is necessary to carry out further clean after the printing. (iii) During the assembly

procedure of the fiber array, it is essential to manually insert slowly to prevent damage. (iv) After the successful insertion of the fiber array, each fiber would be slightly adjusted to achieve the parallel assembly.

- The assembly is finalized by applying UV glue. Has this fixation been tested under different conditions, particularly humidity, which is a significant factor in a clinical context?

Response:

Thanks for your kind comments. The fixation performance of the UV glue has been tested comprehensively. Firstly, we attempted to manually tear the skeleton from the fiber array but failed, confirming the strong fixation of the UV glue. Next, we immersed the assembly in a hydrogel solution to generate the outer hydrogel skin. The skeleton remained well-fixed to the fiber array, further verifying the glue's effectiveness. Additionally, after ex-vivo experiments in a porcine lung bronchial channel environment, the skeleton withstood manual tear tests, demonstrating excellent fixation performance under humid conditions.

We have already added more detailed descriptions of the fixation performance in the supplementary text. Please see the following modifications.

Modifications: (Supplementary Note S1)

Supplementary Note S1. Additional information about the fabrication procedures

Fixation performance of the UV glue: The fixation performance of the UV glue has been tested comprehensively. Firstly, we attempted to manually tear the skeleton from the fiber array but failed, confirming the strong fixation of the UV glue. Next, we immersed the assembly in a hydrogel solution to generate the outer hydrogel skin. The skeleton remained well-fixed to the fiber array, further verifying the glue's effectiveness. Additionally, after ex-vivo experiments in a porcine lung bronchial channel environment, the skeleton withstood manual tear tests, demonstrating excellent fixation performance under humid conditions.

The analytical approach employed in this study is robust, with appropriate use of methods to evaluate the robot's performance. The authors use statistical methods to analyze the data obtained during the robot's performance tests, particularly concerning navigation accuracy and the efficiency of the imaging system. The experimental results show good agreement with the theoretical analyses, which reinforces the validity of the conclusions.

Response:

Thanks again for your positive comments on our work.

Reference

[1] Kiesslich, R., Goetz, M., Hoffman, A., & Galle, P. R. (2011). New imaging techniques and opportunities in endoscopy. *Nature reviews Gastroenterology & hepatology*, *8*(10), 547-553.

[2] Subramanian, V., & Ragunath, K. (2014). Advanced endoscopic imaging: a review of commercially available technologies. *Clinical Gastroenterology and Hepatology*, *12*(3), 368-376.

[3] Choi, W., Kang, M., Hong, J. H., Katz, O., Lee, B., Kim, G. H., ... & Choi, W. (2022). Flexible-type ultrathin holographic endoscope for microscopic imaging of unstained biological tissues. *Nature communications*, *13*(1), 4469.

[4] Gifari, M. W., Naghibi, H., Stramigioli, S., & Abayazid, M. (2019). A review on recent advances in soft surgical robots for endoscopic applications. *The International Journal of Medical Robotics and Computer Assisted Surgery*, *15*(5), e2010.

[5] Song, Y., Wang, S., Luo, X., & Shi, C. (2022). Design and optimization of a 3D printed distal flexible joint for endoscopic surgery. *IEEE Transactions on Medical Robotics and Bionics*, *4*(1), 38-49.

[6] https://www.fiberscope.net/ultra-fine-micro-borescope/

[7] https://aitproducts.com/wiki/flexible_borescope_bending_radius.html

[8] Yang, X., Shang, W., Lu, H., Liu, Y., Yang, L., Tan, R., ... & Shen, Y. (2020). An agglutinate magnetic spray transforms inanimate objects into millirobots for biomedical applications. *Science robotics*, *5*(48), eabc8191.

[9] Loh, J. M., Lim, Y. J. L., Tay, J. T., Cheng, H. M., Tey, H. L., & Liang, K. (2024). Design and fabrication of customizable microneedles enabled by 3D printing for biomedical applications. *Bioactive Materials*, *32*, 222-241.

[10] Xiao, R., Feng, X., Liu, W., Zhou, W., Li, X., Song, I., ... & Lu, Y. (2023). Direct 3D printing of thin-walled cardiovascular stents with negative Poisson's ratio (NPR) structure and functional metallic coating. *Composite Structures*, *306*, 116572.

[11] Cheng, X., Li, W., Yuan, J., & Wang, S. (2023). Simultaneously Enhanced Chain Flexibility, Three Dimensional Printability, and Reduction of Shrinkage Stress in Biodegradable and Photocurable Multiblock Copolymers. *Macromolecules*, *56*(10), 3550-3561.

[12] Zare, M., Ghomi, E. R., Venkatraman, P. D., & Ramakrishna, S. (2021). Silicone-based biomaterials for biomedical applications: antimicrobial strategies and 3D printing technologies. *Journal of applied polymer science*, *138*(38), 50969.

[13] del Bosque, A., Sánchez-Romate, X. F., Gómez, A., Sánchez, M., & Ureña, A. (2023). Highly stretchable strain sensors based on graphene nanoplatelet-doped

ecoflex for biomedical purposes. *Sensors and Actuators A: Physical*, *353*, 114249.

[14] Sparks, J. L., Vavalle, N. A., Kasting, K. E., Long, B., Tanaka, M. L., Sanger, P. A., ... & Conner-Kerr, T. A. (2015). Use of silicone materials to simulate tissue biomechanics as related to deep tissue injury. *Advances in skin & wound care*, *28*(2), 59-68.

[15] Yu, Y., Yuk, H., Parada, G. A., Wu, Y., Liu, X., Nabzdyk, C. S., ... & Zhao, X. (2019). Multifunctional “hydrogel skins” on diverse polymers with arbitrary shapes. *Advanced Materials*, *31*(7), 1807101.

Dear reviewers,

Thank you for your valuable comments concerning our manuscript. The constructive comments do much help to improve the quality of the paper and have been carefully addressed and answered in a point-by-point manner. For the convenience of the reviewers, the comments and suggestions are listed below in the **blue font**, followed by our responses in the normal **black font**. We also highlighted the corresponding modifications in our revised manuscript in the **red font**.

Reviewer #1 (Remarks to the Author):

The authors have addressed most of my comments.

Response:

Thanks for your positive evaluation on our work.

The only final comment I have is for the authors to double check this newly added sentence: "Despite the reported stitching approach would slow down the scanning speed and be prone to body's movements". This sentence is a bit confusing. Did you mean, "Despite these advantages, the reported stitching approach would slow down the scanning speed and be prone to body's movements".

Response:

Thanks for your insightful comments. We acknowledge your suggestions and have improved the description in the revised version to obtain a better understanding. Please see the following modifications.

Modifications: (The second paragraph of Section Discussion))

Due to the inherent contour limitation of the fiber bundle, the field of vision of existing fiber-based imaging systems usually cannot provide sufficient information on the pathological area. Leveraging the probe's high-precision motion, we proposed a strategy of local scanning and stitching, enlarging the overall imaging region by ~25 folds. This strategy not only enhances the diagnostic potential of the robot through scanning imaging of pathological areas but also opens up possibilities for precise in situ surgical manipulations. Despite these advantages, the reported stitching approach here would potentially slow down the scanning speed and be prone to body's movements. In this manuscript, we have demonstrated the feasibility of this approach for enlarging the imaging area. In future work, we will address this challenge by: optimizing the image processing algorithm to enhance stitching efficiency; designing the scanning path as a denser spiral trajectory with smaller gaps between adjacent curves to minimize information loss; and upgrading the stitching algorithm by integrating both trajectory and image features to improve accuracy.

Reviewer #3 (Remarks to the Author):

I would like to thank the authors for their detailed responses to my previous comments. The points raised have been addressed appropriately, and the revisions made to the manuscript (Supplementary Materials) seem coherent to me.

Response:

Thanks for your comprehensive evaluation on our work.